ACS APPLIED MATERIALS & INTERFACES

www.acsami.org

Research Article

Processing–Structure–Performance Relationships of Microporous Metal–Organic Polymers for Size-Selective Separations

Jen-Yu Huang, Yuanze Xu, Phillip J. Milner, and Tobias Hanrath*

Cite This: *ACS Appl. Mater. Interfaces* 2021, 13, 3521–3527

Read Online

ACCESS | Metrics & More | Article Recommendations | Supporting Information

ABSTRACT: Small-molecule impurities, such as *N*-nitrosodimethylamine (NDMA), have infiltrated the generic drug industry, leading to recalls in commonly prescribed blood pressure and stomach drugs in over 43 countries since 2018 and directly affecting tens of millions of patients. One promising strategy to remove small-molecule impurities like NDMA from drug molecules is by size exclusion, in which the contaminant is removed by selective adsorption onto a (micro)porous material due to its smaller size. However, current solution-phase size-exclusion separations are primarily limited by the throughput-selectivity trade-off. Here, we report a bioinspired solution to conquer these critical challenges by leveraging the assembly of atomically precise building blocks into hierarchically porous structures. We introduce a bottom-up approach to form micropores, mesopores, and macroscopic superstructures simultaneously using functionalized oxozirconium clusters as building blocks. Further, we leverage recent advances in photopolymerization to design macroscopic flow structures to mitigate backpressure. Based on these multiscale design principles, we engineer simple, inexpensive devices that are able to separate NDMA from contaminated drugs. Beyond this urgent model system, we expect this design strategy to open up hitherto unexplored avenues of nanomaterial superstructure fabrication for a range of size-exclusion purification strategies.

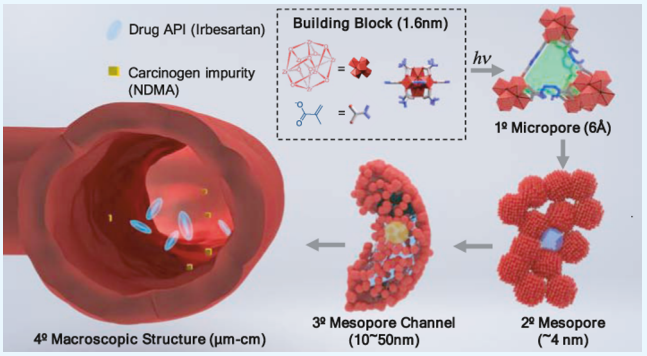

KEYWORDS: *metal-organic polymers, N-nitrosodimethylamine (NDMA), micropores, mesopores, macroscopic*

INTRODUCTION

Microporous materials possess important potential technological implications spanning storage, separation, and catalysis.[1] However, the absence of monolithic forms significantly limits their mass transportation and thus practical applications.[2,3] In general, separations using microporous materials are carried out using powdered materials in a low-throughput manner, leading either to a throughput-selectivity trade-off or high back pressures.[4] Notably, high throughput and selectivity can be achieved simultaneously in natural systems by hierarchical design.[5] For example, intestines utilize macroporous channels to enable the transport of nutrients and nanopores to enable adsorption of these nutrients. In fact, a similar strategy was adopted in the design of a metal–organic framework (MOF) membrane. By loading MOFs in highly porous polymer matrix with micron- and nanosized channels, the matrix materials were demonstrated to access the merits of high permeability and selectivity.[6,7] Nonetheless, our ability to fabricate microporous materials into structures analogous to natural hierarchical design is still in its infancy.

Concurrent advances in the nanostructured building blocks[8,9] and optical patterning[10] have opened opportunities to program materials over multiple length scales. The assembly of colloidal nanoparticles is an attractive strategy to produce hierarchical structures.[11−13] Studies using molecular ligand–ligand interactions, such as organic ligands or DNA, to directionally bind and orientate nanobuilding blocks have generated nanoscale features including mesopores and macropores.[14−16] On the other hand, advances in photoresponsive ligand chemistries have created new prospects to spatially pattern assemblies by light.[17,18] Recent works have demonstrated the fabrication of hierarchical nanoporous materials by combining nanoparticles' assemblies with light-initiated three-dimensional (3D) printing.[19−21] Unfortunately, this strategy has so far not been realized for the formation of microporous materials, as the length of ligands and their polymerization limit our capability to generate sub-nanometer features.

The ability to design and implement hierarchically porous materials presents compelling prospects to address challenging purifications.[22] Combining intrinsic micropores for host–guest interactions with interconnected meso/macropores for en-

Received: August 17, 2020
Accepted: January 4, 2021
Published: January 13, 2021

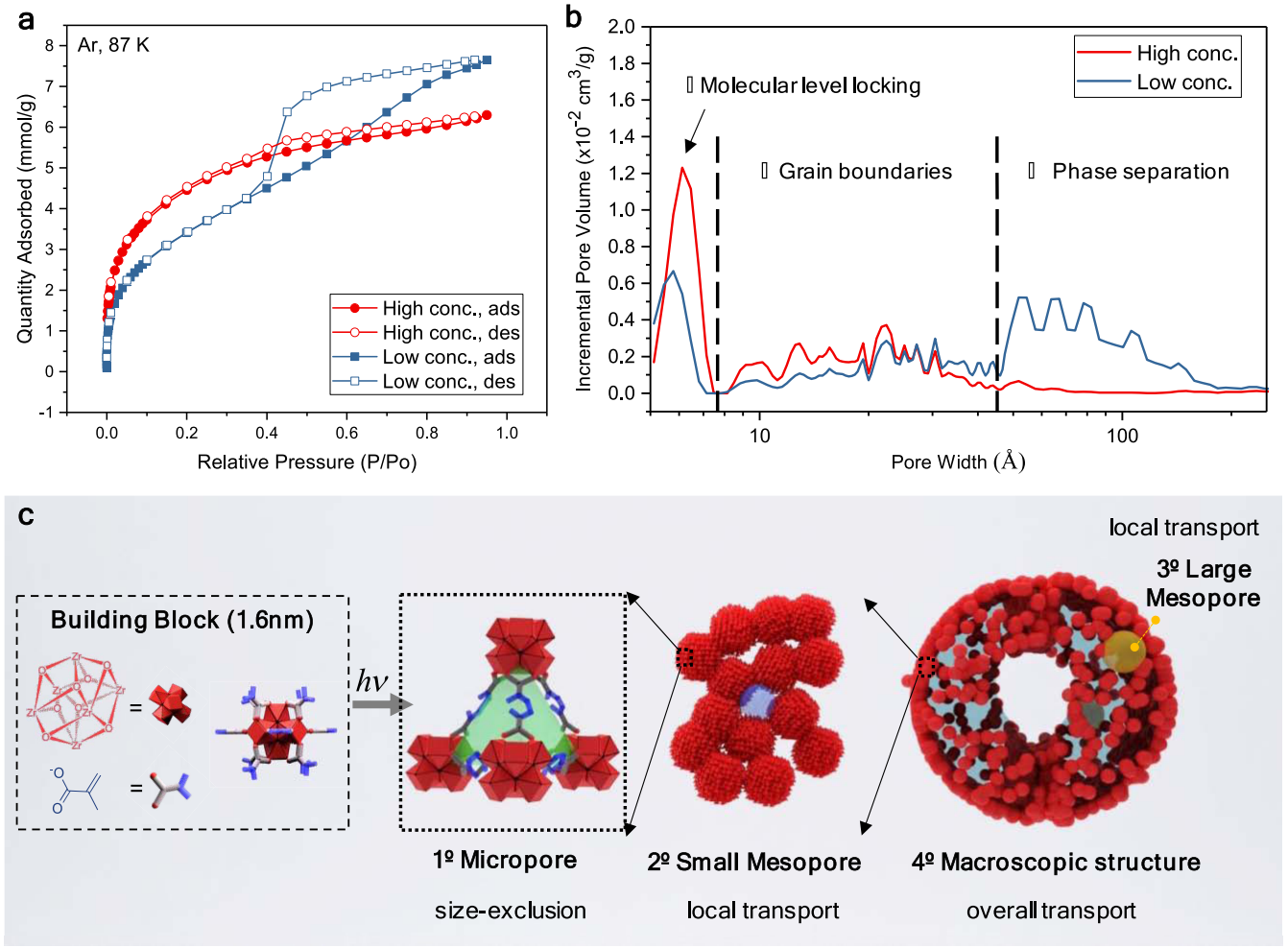

Figure 1. Gas adsorption measurement and multiscale pore-size analysis. (a) Argon sorption isotherms with samples prepared in high and low concentration of building units, 500 and 100 mg/mL of Zr-MAA, respectively. (b) Pore-size distributions of the two samples in (a). The mechanisms of pore formation are different for regions I, II, and III. (c) Proposed hierarchy of multiscale porosities by leveraging assemblies of nanobuilding blocks to form around 6 Å micropores, 2−3 nm and tens of nm mesopores; and light-based additive manufacturing to define macroscopic features, such as a mm scale hollow channel.

hanced mass transport can uniquely open up high-resolution size-selective separations. One specific and urgent separation challenge that could benefit from this approach is the removal of carcinogenic contaminants from generic pharmaceuticals.[23] *N*-nitrosodimethylamine (NDMA), a member of the *N*-nitrosamine family and a potent carcinogen, has been discovered in multiple generic drugs including angiotensin II receptor blockers (e.g., irbesartan, valsartan), ranitidine, and potentially metformin.[24,25]

Conventional approaches fall short of addressing the challenge of removing NDMA from pharmaceuticals. NDMA is resistant to air stripping due to its high solubility and polarity.[24] In addition, commonly used strategies of separation based on ion strength or hydrophobic interaction are both ineffective because nitrosamines are neutral at pH ranging from 4 to 10 and have weakly hydrophobic interactions with sorbents.[24] Last, current size-exclusion separations are primarily limited to larger molecular weight species (>10 kDa) and do not provide enough resolution to remove NDMA from other small molecules. Therefore, new strategies are needed for the selective removal of NDMA from contaminated pharmaceuticals.

Here, we present our findings to accomplish hierarchical control over microscopic porosity, mesoscale assembly, and macroscopic superstructures, which leads to new strategy achieving efficient mass transport and selective adsorption of small molecular impurities, such as NDMA. In our recent work, we observed several nanometers and tens of nanometer mesopores formed by the assemblies of photoresponsive zirconia clusters.[20] However, the mechanism of pore formation and its relationship with assemblies were not realized. Therefore, we conducted detailed studies by tuning the processing conditions and probing the material with multiple gas species. Surprisingly, in addition to previously reported disordered mesopores, we observe the directional connection of colloidal building blocks at the molecular level to generate micropores. The observation extends the feature size of nanoparticles' assemblies and highlights the importance of atomic-resolution nanobuilding blocks. Furthermore, we validate the formation of sub-nm pores and leverage the capability of hierarchical fabrication to demonstrate the efficient removal of NDMA from the drug Irbesartan. This promising technique enables control of pore size on the ångström level as an alternative to the recent focus on tuning chemical functionalities to separate species by polarity.[26] We

https://dx.doi.org/10.1021/acsami.0c14827
ACS Appl. Mater. Interfaces 2021, 13, 3521−3527

elucidate the underlying relationship between processing (cluster concentration), structure (pore-size distribution), and performance (size-selective separation) to produce next-generation hierarchically porous materials.

RESULTS AND DISCUSSION

We employ the Zr_6 methacrylate-functionalized cluster $Zr_6O_4(OH)_4(MAA)_{12}$ (Zr-MAA) as a colloidal building block to prepare hierarchical micro/mesoporous materials. The characterization of Zr-MAA is summarized in Figure S1. After synthesis, Zr-MAA was prepared as a photoresponsive "ink" by dissolving into toluene along with a photoinitiator (diphenyl(2,4,6-trimethylbenzoyl) phosphine oxide). Exposing this formulation to ultraviolet (UV) light locally triggers polymerization of the methacrylate groups and forms robust connections between constituent building blocks, creating a micro/mesoporous monolith with designed shapes. The cross-linking of methacrylate groups is supported by Fourier transform infrared (FTIR) measurements before and after light exposure (Figure S3). The assemblies of building blocks determine features in atomic-scale to nanoscale, such as micropores and mesopores. On the other hand, the macroscopic design is defined by light-based additive manufacturing strategies, such as moldings or patterned UV light sources. As a demonstration, we printed a macroscopic pattern using the Zr-MAA ink with a digital light processing projector as shown in Figure S2. We patterned the projection of a text, demonstrating the shape-control capabilities offered by this technique.

The materials fabricated using our approach share some similarities with porous coordination polymers (PCP).[26−28] For PCP, micropores are formed via the connection of multidentate organic linkers with inorganic cores. However, the inherent fragility of pores limits the synthesized microporous materials to a powdered form, leading to notoriously challenging processing. In an important distinction from prior work regarding PCP, we designed the building blocks based on monodentate ligands ending with photoresponsive groups (C═C) instead of active chelating groups. Therefore, the synthesized building blocks are stable and processable in solvents before any pores have formed. Then, they can later be reacted into a hierarchically micro/mesoporous monolith in a single step by photoinitiated polymerization.

We analyzed the surface area and pore-size distribution using Ar gas adsorption (Figure 1). The two samples were fabricated with high and low concentration of Zr-MAA inks, 500 and 100 mg/mL, respectively. The Brunauer−Emmett−Teller (BET) surface area of the high concentration sample is 349 ± 2 m^2/g (Langmuir surface area: 577 ± 2 m^2/g). On the other hand, the BET surface area of the low concentration sample is 287 ± 3 m^2/g (Langmuir surface area: 718 ± 39 m^2/g). The BET surface areas are quite similar, indicating similar amounts of microporous regimes. However, the Langmuir surface area of the low concentration sample is higher, indicating it has a higher totally accessible pore volume. The step-like desorption behavior of the isotherm in Figure 1a is indicative of mesopores within the material. Further, we simulated the pore-size distribution using a NLDFT model, assuming the adsorption of Argon on an oxide surface at 87 K within cylindrical pores. Figure 1b shows the hierarchy of pore sizes spanning from Å sized micropores (region I), several nm (region II) to tens of nm (region III) sized mesopores. The first distribution is in the micropore regime (6 Å), most likely arises due to the connection of building blocks similar to the structure of the PCP UiO-66.[29] Importantly, the observed micropores unveil an unreported chemistry to utilize acrylate monomer ligands to attach inorganic nanoparticles, which is different from bulky photopolymerization. The 6 Å pores can be referred to as tetrahedral cages similar to the tetrahedral cages of UiO-66;[29,30] however, we cannot rule out the formation of octahedra at this time. We infer that the kinetics to form tetrahedral cages are faster than forming octahedral cages, so the building units incline to stack into tetrahedra (Figure S4).

The second pore-size distribution is around 2−3 nm. We attribute these pores to the space between superclusters of linked tetrahedra; the superclusters visible in scanning electron microscopy images are around tens of nanometers in diameter (Figure S5). The distribution of sub-nm pores (within the tetrahedron) and nm pores (between the superclusters) hence reflects the nucleation and growth conditions. The growth of Zr-MAA nanoclusters into a single, large crystal is difficult because of the relatively fast kinetics and irreversibility.

The third pore-size distribution is in the range of ten nanometers, which we attribute to phase separation behavior during material processing. Large mesopores like the ones formed here have been previously observed using the same $[Zr_6O_4(OH)_4]^{12+}$ cluster under hydrothermal conditions.[31]

The relationship between the broad spectrum of pore sizes is schematically summarized in Figure 1c. We show that the pore-size distribution can be adjusted by changing the building block concentration. We hypothesize that this processing−structure relationship derives from the underlying nucleation and growth dynamics of the tetrahedra and superclusters. A high concentration of building blocks leads to enhanced nucleation of superclusters, whereas the low concentration of Zr-MAA leads to less nucleation and more growth to form larger superclusters and hence a more dominant contribution of nm pores in the final material. The ability to control hierarchical porosity can greatly mitigate mass transfer limitations, increasing the likelihood of small-molecule adsorption in the micropores.

To further validate the permanent porosity and utility of pores for size-selective separations, we probed the adsorption of different gases. Carbon dioxide (~2−3 Å) uptake was measured (Figure S7a). The result confirms that the sample made from a high concentration of Zr-MAA can uptake more CO_2 because of more micropores. However, both of the samples possess relatively low CO_2 capacity (<0.4 mmol/g) due to the absence of strong CO_2 binding sites. Complementary gas uptake experiments with toluene (~5−6 Å) conducted reveal a gas uptake (~3 mmol/g) that is 7 times higher compared to CO_2. Due to toluene's increased ability to participate in van der Waal's interactions with the pore walls, toluene adsorbs more strongly than CO_2 in both materials. Toluene interacts more strongly with the pore walls than CO_2, so it can likely be trapped more strongly within the 6 Å micropores (Figure S7b).

Having established the relationship between processing conditions and pore-size distribution, we set out to test the performance in chemical separation applications. The targeted molecular structure and computed 3D model of NDMA and Irbesartan are shown in Figure S10. The fabrication of these mesoscale porous materials can be combined with light processing approaches to create structures in which flow channels can be defined from the μm to cm scale. We started by printing a micro/mesoporous monolith fully in a syringe

https://dx.doi.org/10.1021/acsami.0c14827
ACS Appl. Mater. Interfaces 2021, 13, 3521−3527

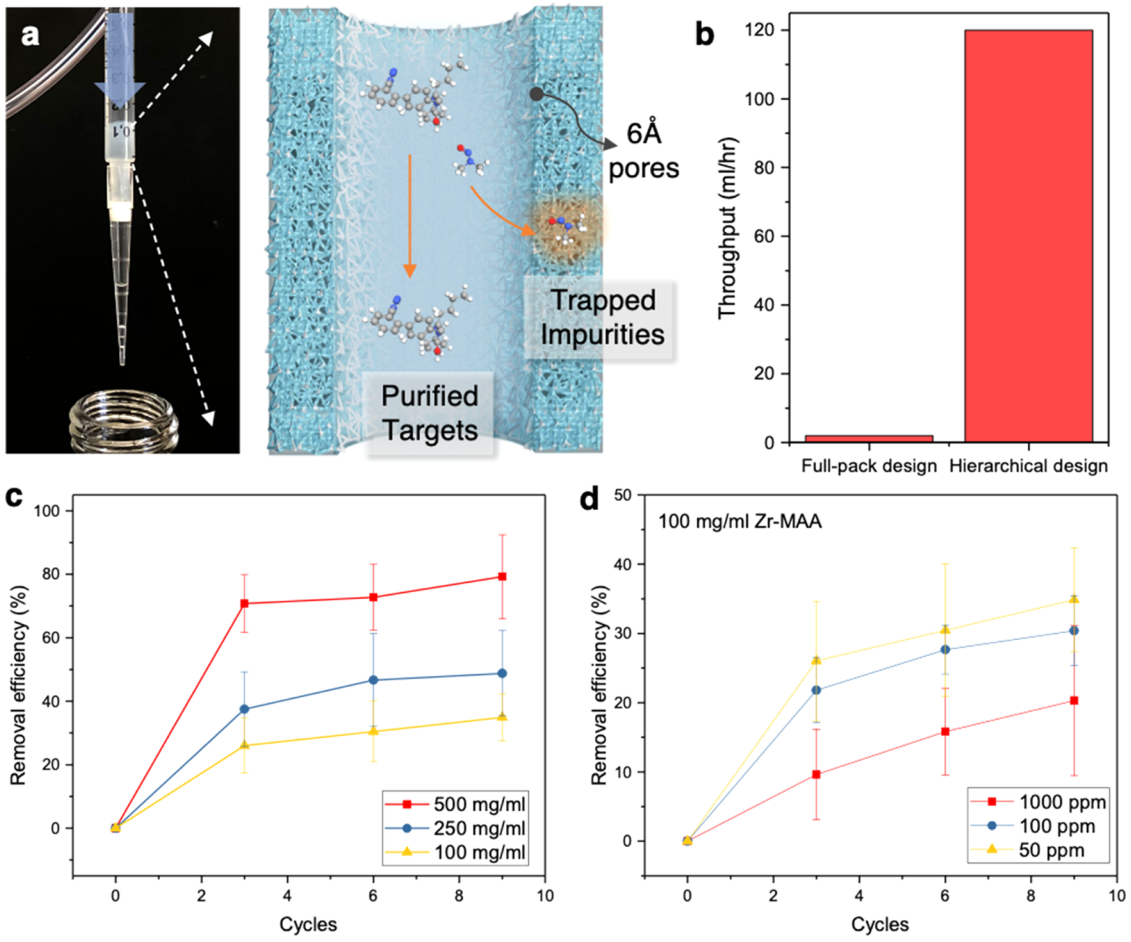

Figure 2. Size-selective separations with hierarchical design. (a) Device setups for the carcinogen removal in recently recalled drugs: syringe filled with superstructures (zoomed in on right). (b) Throughput comparison of hierarchical design and full pack design columns. Removal efficiency of (c) columns prepared with different concentrations of Zr-MAA and (d) different initial concentrations of NDMA contaminates.

similar to a solid phase extraction setup. Separation experiments to remove NDMA showed a reduction in the carcinogen level from 5% in the inlet feed to 0% in the outlet (Figures S11 and S12), which validates the use of superstructures for size-selective separation. However, even given the exceptional hierarchy of large and small mesopores to help transportation, the flow rate through monolithic structures is still limited to around 1−2 mL/h due to high back pressures, which is the critical bottleneck for almost all separation technologies.

We leveraged the freedom to fabricate complex shapes using our proposed processing method to explore different macroscopic structures to resolve the backpressure challenge. Inspired by the hierarchical design present in nature, we adopted a structure similar to that of an intestine. This more efficient design increases the flow rate from mL/h to mL/min. A hollow tube superstructure (akin to a hollow-fiber membrane commonly used in separation processes) was fabricated with the macroscopic channel for transportation, and the wall was used liked villi to absorb impurities (Figures 2a and S9). Figure 2b concludes the improvement in throughput by hierarchical design compared with the common fully packed design. The removal efficiencies of hierarchically designed superstructures prepared with different concentrations of Zr-MAA are studied in Figure 2c. Higher concentrations of Zr-MAA precursor show better removal efficiency. The result is consistent with gas-phase studies supporting that more micropores help the separation performance. The optimized superstructure shows averagely 80% NDMA removal efficiency after nine cycles, bringing the concentration down from an initial 50 ppm to around 10 ppm, at a flow rate of 2 mL/min, which is tens of times faster than the fully packed design.

We examined the removal efficiency with different initial NDMA concentrations (Figure 2d) and a simplified analytical model (Supporting Information (SI) Section 7) to explain the boundary layer phenomenon. Notably, the maximum adsorption capacity was around 0.1 mmol of NDMA/g of Zr-MAA. However, after nine cycles of separation with 1000 ppm initial concentration, only 0.0027 mmol of NDMA was captured in the device with 150 mg of Zr-MAA. The used capacity is only 0.018 mmol of NDMA/g of Zr-MAA. The results suggest that only 18% of micropores were used in this configuration and there are room to tune the macroscopic design to better utilize all micropores. This highlights the importance and potential to achieve contradicting throughput and performance at the same time by rationally designing in macroscopic scale. To date, relatively few studies have taken macroscopic design into consideration because of the insufficient processing approaches available.[4]

We tested the yield and performance in the separation of the NDMA from a recalled batch of pharmaceuticals as shown in Figure 3. On average, the recalled drugs surpass the FDA

https://dx.doi.org/10.1021/acsami.0c14827
ACS Appl. Mater. Interfaces 2021, 13, 3521−3527

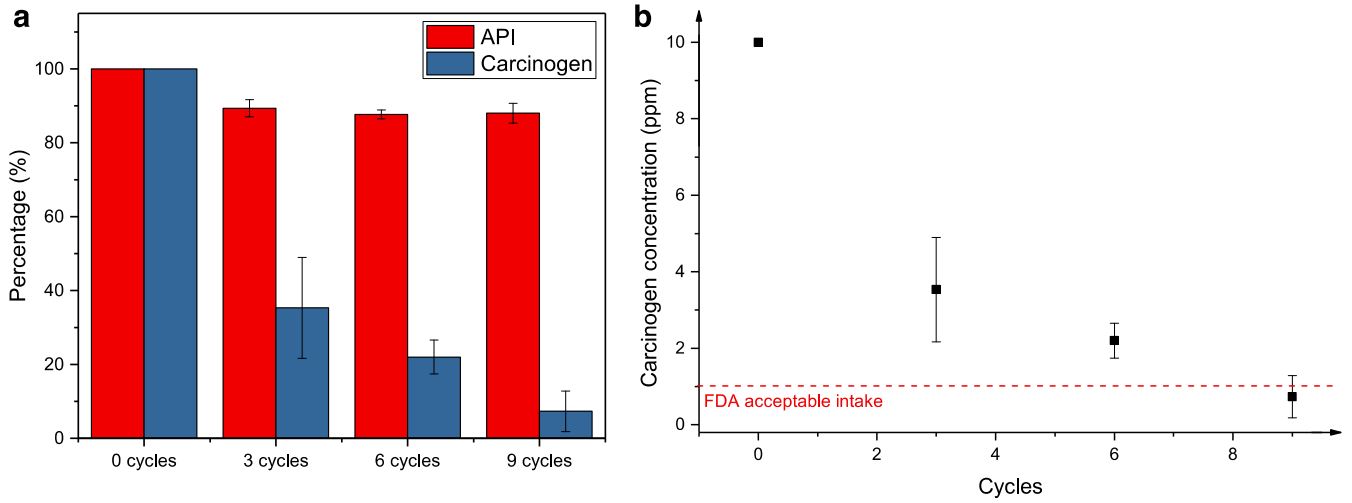

Figure 3. Contaminant removal efficiency. (a) Yield of separating drug API and carcinogen impurity with our hierarchical micro/mesoporous device under different separation cycles. (b) Carcinogen concentration after a given number of separation cycles.

approved intake amount by more than 10 times the limit. Thus, we did experiments with a mixture containing the Irbesartan drug and 10 ppm NDMA. The contaminates drop below FDA's average requirement, 1 ppm, after nine cycles of separation with a 0.5 cm device shown in Figure 3b. The overall separation time was less than 3 min, where each cycle only took around 10 s. Notably, the device can be further optimized to cut cycles by either increase the length or decrease the inner diameter of the device based on our analytical calculation. In addition, the separation configuration can be potentially set up continuously. More importantly, the result was achieved selectively with only a ~10% loss in the drug yield, as shown in Figure 3a.

Our hierarchical device demonstrates a unique opportunity for "structured" microporous materials to become an energy-efficient, cost-effective, and high-selective alternative for molecular separation processes. With the distinguishing features of solution processability in room temperature and selected low-cost precursors, the device can be fabricated on-demand within minutes and tens of dollars. In addition to its simplicity, the device is readily adaptable for potential use in various pharmaceutical scenarios, such as an additional/combined processing step of chromatography or tangential flow filtration. More importantly, although we only showed a simple hollow structure, we envision that exploration in arbitrary shapes can lead to the optimized area for mass transfer, a higher flow capacity, and a lower pressure drop analogy to the development of trays for distillation and packed columns from random to structured packings.

CONCLUSIONS

We demonstrate how hierarchical control over microscopic porosity, mesoscale assembly, and macroscopic superstructures leads to new materials exhibiting efficient mass transport and size-selective adsorption of small-molecule contaminants. Beyond the specific model system of NDMA removal in a hollow-fiber flow geometry, we envision that the concurrent advances in materials synthesis and photoprocessing[20] enable a diverse range of hierarchical porous structures in which mass transport and adsorption can be independently optimized. The emerging opportunities to assemble nanobuilding blocks to control spacing and architectures from ångström to centimeter scales by design allow for theorists and experimentalists to design and test novel porous materials. Hierarchically porous materials shown here solve recent challenges in attaining high purity and high flow rate at the same time. Given the broad library of inorganic cores, we foresee that this approach will inspire a number of novel device architectures. Our results and the hierarchical strategy proposed herein pave the way for practical usages of structured microporous materials in emerging separation applications.

METHODS

Building Block Synthesis. Zr-MAA was synthesized by the modified method previously reported.[32] Briefly, 1 mL of Zr isopropoxide was mixed with 1 mL of methacrylic acid in a flask. The flask was left opened for solvent evaporation to one-half of the initial volume, and the product was washed with 1-propanol. The final product was dried under vacuum.

Fabrication of Superstructures. Ink was formulated by mixing dried Zr-MAA clusters from the previous step with a photoinitiator and solvent. For example, 100 mg of synthesized Zr-MAA, 1 mg of photoinitiator, diphenyl(2,4,6-trimethylbenzoyl) phosphine oxide, were added into 1 mL of toluene. Inks were purged with nitrogen flow for 2 min before usage. Samples for gas sorption measurements were prepared by a digital light processing projector operating with 385 nm wavelength light and intensities of about 10 mW/cm^2. Free-standing monoliths formed as a single layer by projecting the light pattern for 2 min directly on top of the Si wafer. Inks with 500 and 100 mg/mL of Zr-MAA were labeled as a high and low concentration in Figure 1.

General Characterization Methods. Powder X-ray diffraction characterization was carried out on Bruker-AXS D8 Discover diffractometer using Cu Kα radiation at λ = 1.54 Å by depositing powder onto a glass substrate. The FTIR was conducted on Bruker Hyperion FT-IR spectrometer and microscope. A background scan was collected before each measurement (64 scans), sample scan was an average of 64 scans, and resolution was set 4 with a data spacing of 0.482 cm^{-1}. The concentration of NDMA carcinogen was measured by Shimadzu 2030 gas chromatography (GC) following the FDA's method. Generally, samples were held at 50 °C for 2 min, ramped from 40 to 100 °C at 5 °C/min, ramped from 100 to 220 °C at 20 °C/min, ramped from 220 to 250 °C at 30 °C/min, and then held at 250 °C for 2 min. ^{1}H NMR spectra were recorded on a Bruker AV500 spectrometer with 16 scans and 45° excitation pulse. NMR data was analyzed by MestReNova.

Gas Sorption. Samples for gas sorption were washed and exchanged with methanol for 24 h. Then, samples were dried with

https://dx.doi.org/10.1021/acsami.0c14827
ACS Appl. Mater. Interfaces 2021, 13, 3521−3527

a supercritical carbon dioxide dryer (Leica CPD300 critical point dryer). Gas adsorption measurements were carried out using a Micromeritics 3-flex gas sorption analyzer and high-purity Ar or CO_2 (99.999% pure). The pore-size distribution was modeled with the cylinder pore DFT based on Ar adsorption on metal oxides.

Liquid-Phase Separation. Ink with different concentrations of Zr-MAA was loaded into a cylindrical plastic tube and then exposed with UV light (385 nm, 10 mW/cm^2) for 5 min. For hierarchical design devices, the ink was injected into a cylindrical plastic tube (diameter 5 mm) with a needle (diameter 1.5 mm) inserted in the middle (Figure S8). Then, the tube was exposed to UV light. Once the superstructure formed, the needle was removed and the device was connected to a syringe pump. A cross-sectional view of the developed device is shown in Figure S9 (inner diameter ∼ 1.8 mm; outer diameter ∼ 5 mm). To clean the superstructure, ethanol was continuously flowing through and the UV−vis spectrum of the outlet flow was monitored. After the absorption peak of unreacted clusters and toluene reduced to zero, a mixture of API and NDMA was flowed through the superstructure iteratively and sampled. For example, a 5 mL of ethanol solution of API (2 mg/mL) and NDMA (0.01 mg/mL) was flowed iteratively through the as-prepared column at a flow rate of 2 mL/min. After the outflow is collected, it was injected back into the column for another cycle. Every cycle, 100 μL was taken from the collected outflow for quantitative GC tests. Experiments were triplicated and columns were not washed between cycles. The maximum capacity was measured by immersing printed Zr-MAA (500 mg/mL) in a 1.2 mL of ethanol solution with 4.8 mg of NDMA for 24 h. After 24 h, 100 μL of the solution was collected for GC test.

Yield calculation.

The concentration of drug was calculated with internal standard (TMS) by NMR

$$\text{concentration}_A = \frac{\text{integral}_A/N_A}{\text{integral}_{TMS}/N_{TMS}} \times \text{concentration}_{TMS}$$

The concentration of carcinogen was calculated with internal standard (dodecane) by GC

$$\text{concentration}_B = \frac{\text{integral}_B}{\text{integral}_{dodecane}} \times \text{concentration}_{dodecane}$$

The yield was calculated based on the initial concentration of each batch of runs.

■ ASSOCIATED CONTENT

Supporting Information

The Supporting Information is available free of charge at https://pubs.acs.org/doi/10.1021/acsami.0c14827.

Characterization of building blocks and their assemblies (PXRD, FTIR, NMR, SEM, and TEM), BET consistency and gas sorption (carbon dioxide and toluene), device fabrication, additional separation studies, and analytical model (PDF)

■ AUTHOR INFORMATION

Corresponding Author

Tobias Hanrath − *Robert F. Smith School of Chemical and Biomolecular Engineering, Cornell University, Ithaca, New York 14853, United States;* orcid.org/0000-0001-5782-4666; Email: tobias.hanrath@cornell.edu

Authors

Jen-Yu Huang − *Robert F. Smith School of Chemical and Biomolecular Engineering, Cornell University, Ithaca, New York 14853, United States;* orcid.org/0000-0003-1906-7857

Yuanze Xu − *Robert F. Smith School of Chemical and Biomolecular Engineering, Cornell University, Ithaca, New York 14853, United States*

Phillip J. Milner − *Department of Chemistry and Chemical Biology, Cornell University, Ithaca, New York 14853, United States;* orcid.org/0000-0002-2618-013X

Complete contact information is available at: https://pubs.acs.org/10.1021/acsami.0c14827

Notes

The authors declare no competing financial interest.

■ ACKNOWLEDGMENTS

J.-Y.H. and T.H. acknowledge support from NSF-CMMI 1635433. This work made use of the Cornell Center for Materials Research Shared Facilities, which are supported through the NSF MRSEC program (DMR-1719875).

■ REFERENCES

(1) Yang, X.-Y.; et al. Hierarchically Porous Materials: Synthesis Strategies and Structure Design. *Chem. Soc. Rev.* **2017**, *46*, 481−558.

(2) Mohammed, A. K.; et al. Connecting Microscopic Structures, Mesoscale Assemblies, and Macroscopic Architectures in 3D-Printed Hierarchical Porous Covalent Organic Framework Foams. *J. Am. Chem. Soc.* **2020**, *142*, 8252−8261.

(3) Jeong, G.-Y.; et al. Metal-organic Framework Patterns and Membranes with Heterogeneous Pores for Flow-assisted Switchable Separations. *Nat. Commun.* **2018**, *9*, No. 3968.

(4) Van de Voorde, B.; Bueken, B.; Denayer, J.; De Vos, D. Adsorptive Separation on Metal−organic Frameworks in The Liquid Phase. *Chem. Soc. Rev.* **2014**, *43*, 5766−5788.

(5) Shen, Y.-X.; et al. Achieving High Permeability and Enhanced Selectivity for Angstrom-scale Separations Using Artificial Water Channel Membranes. *Nat. Commun.* **2018**, *9*, No. 2294.

(6) Wang, H.; et al. Membrane Adsorbers with Ultrahigh Metal-organic Framework Loading for High Flux Separations. *Nat. Commun.* **2019**, *10*, No. 4204.

(7) Denny, M. S., Jr.; Cohen, S. M. In Situ Modification of Metal-Organic Frameworks in Mixed-Matrix Membranes. *Angew. Chem., Int. Ed.* **2015**, *54*, 9029−9032.

(8) Sanchez, C.; et al. Designed Hybrid Organic−Inorganic Nanocomposites from Functional Nanobuilding Blocks. *Chem. Mater.* **2001**, *13*, 3061−3083.

(9) kovalenko, M. V.; et al. Prospects of Nanoscience with Nanocrystals. *ACS Nano* **2015**, *9*, 1012−1057.

(10) Corrigan, N.; Yeow, J.; Judzewitsch, P.; Xu, J.; Boyer, C. A. J. M. Seeing the Light: Advancing Materials Chemistry through Photopolymerization. *Angew. Chem.* **2019**, *131*, 5224−5243.

(11) Rozes, L.; Sanchez, C. Titanium Oxo-clusters: Precursors for a Lego-like Construction of Nanostructured Hybrid Materials. *Chem. Soc. Rev.* **2011**, *40*, 1006−26.

(12) Phillips, K. R.; et al. A Colloidoscope of Colloid-based Porous Materials and Their Uses. *Chem. Soc. Rev.* **2016**, *45*, 281−322.

(13) Nicole, L.; Rozes, L.; Sanchez, C. Integrative Approaches to Hybrid Multifunctional Materials: From Multidisciplinary Research to Applied Technologies. *Adv. Mater.* **2010**, *22*, 3208−3214.

(14) Guo, J.; et al. Modular Assembly of Superstructures from Polyphenol-functionalized Building Blocks. *Nat. Nanotechnol.* **2016**, *11*, 1105−1111.

(15) Hu, Y.; Niemeyer, C. M. From DNA Nanotechnology to Material Systems Engineering. *Adv. Mater.* **2019**, *31*, No. e1806294.

(16) Nicole, L.; Laberty-Robert, C.; Rozes, L.; Sanchez, C. Hybrid Materials Science: A Promised Land for the Integrative Design of Multifunctional Materials. *Nanoscale* **2014**, *6*, 6267−6292.

(17) Gao, Y.; Huang, J.-Y.; Balazs, D. M.; Xu, Y.; Hanrath, T. Photoinitiated Transformation of Nanocrystal Superlattice Poly-

morphs Assembled at a Fluid Interface. *Adv. Mater. Interfaces* **2020**, *7*, No. 2001064.
(18) Wang, Y.; Fedin, I.; Zhang, H.; Talapin, D. V. Direct Optical Lithography of Functional Inorganic Nanomaterials. *Science* **2017**, *357*, 385−388.
(19) Halevi, O.; et al. Synthesis through 3D printing: Formation of 3D Coordination Polymers. *RSC Adv.* **2020**, *10*, 14812−14817.
(20) Huang, J.-Y.; et al. Three-Dimensional Printing of Hierarchical Porous Architectures. *Chem. Mater.* **2019**, *31*, 10017−10022.
(21) Aubert, T.; Huang, J.-Y.; Ma, K.; Hanrath, T.; Wiesner, U. Porous Cage-derived Nanomaterial Inks for Direct and Internal Three-dimensional Printing. *Nat. Commun.* **2020**, *11*, No. 4695.
(22) Zhao, X.; Wang, Y.; Li, D.-S.; Bu, X.; Feng, P. Metal-Organic Frameworks for Separation. *Adv. Mater.* **2018**, *30*, No. 1705189.
(23) Snodin, D. J.; Elder, D. P. Short Commentary on NDMA (N-nitrosodimethylamine) Contamination of Valsartan Products. *Regul. Toxicol. Pharmacol.* **2019**, *103*, 325−329.
(24) Sgroi, M.; Vagliasindi, F. G. A.; Snyder, S. A.; Roccaro, P. N-Nitrosodimethylamine (NDMA) and its Precursors in Water and Wastewater: A Review on Formation and Removal. *Chemosphere* **2018**, *191*, 685−703.
(25) Information about Nitrosamine Impurities in Medications. https://www.fda.gov/drugs/drug-safety-and-availability/information-aboutnitrosamine-impurities-medications 1−3, 2020.
(26) Van de Voorde, B.; Bueken, B.; Denayer, J.; De Vos, D. Adsorptive Separation on Metal−organic Frameworks in the Liquid Phase. *Chem. Soc. Rev.* **2014**, *43*, 5766−5788.
(27) Foo, M.L.; Matsuda, R.; Kitagawa, S. Functional Hybrid Porous Coordination Polymers. *Chem. Mater.* **2014**, *26*, 310−322.
(28) Furukawa, H.; et al. Water Adsorption in Porous Metal−Organic Frameworks and Related Materials. *J. Am. Chem. Soc.* **2014**, *136*, 4369−4381.
(29) Hon Lau, C.; Babarao, R.; Hill, M. R. A Route to Drastic Increase of CO_2 Uptake in Zr Metal Organic Framework UiO-66. *Chem. Commun.* **2013**, *49*, 3634−3636.
(30) Bambalaza, S. E.; et al. Compaction of a Zirconium Metal−organic Framework (UiO-66) for High Density Hydrogen Storage Applications. *J. Mater. Chem. A* **2018**, *6*, 23569−23577.
(31) Bueken, B.; et al. Gel-based Morphological Design of Zirconium Metal−organic Frameworks. *Chem. Sci.* **2017**, *8*, 3939−3948.
(32) Užarević, K.; et al. Mechanochemical and Solvent-free Assembly of Zirconium-based Metal−organic Frameworks. *Chem. Commun.* **2016**, *52*, 2133−2136.

https://dx.doi.org/10.1021/acsami.0c14827
ACS Appl. Mater. Interfaces 2021, 13, 3521−3527